Thermal Dissociation Kinetics of Solid and Liquid Ammonium Nitrate

Sergey Vyazovkin,* Jacalyn S. Clawson, and Charles A. Wight*

Center for Thermal Analysis, Department of Chemistry, University of Utah 315 S., 1400 E, Salt Lake City, Utah 84112

Received September 5, 2000. Revised Manuscript Received November 18, 2000

Thermogravimetry has been used to study the kinetics of the thermal dissociation of solid and liquid ammonium nitrate. Model-fitting and model-free kinetic methods have been applied to the sets of isothermal and nonisothermal measurements to derive kinetic characteristics of the processes. The application of the model-fitting method to the isothermal data has demonstrated that both solid- and liquid-phase kinetics are characterized by a single activation energy of ∼90 kJ mol^{-1} and by the model of a contracting cylinder. A model-free isoconversional method has also been applied to isothermal and nonisothermal data and has yielded an activation energy of ∼90 kJ mol^{-1}, which is essentially independent of the extent of conversion. The obtained kinetic characteristics have been assigned to the process of dissociative sublimation/vaporization.

Introduction

Ammonium nitrate (AN) finds a widespread application as both fertilizer and energetic material. As an energetic material, AN has inspired numerous decomposition studies at elevated temperatures. Obtaining information relevant to combustion requires the use of fast heating rates. By using fast heating (130 K s^{-1}) and temperature jump (2000 K s^{-1}) techniques, Brill et al.[1,2] have studied the thermal decomposition of AN at temperatures up to 600 °C. Even higher temperatures have been reached by Pasternack and Rice[3] in their laser ablation studies of AN. On the other hand, slow heating techniques (<1 K s^{-1}), such as thermogravimetric analysis (TGA), and differential scanning calorimetry (DSC) enable thermal decompositions to be studied at moderately elevated temperatures. These techniques are an invaluable tool for estimating the thermal stability of energetic materials under conditions of manufacture, handling, and storage. Such estimates are primarily concerned with the temperature dependence of the reaction rate. Because the temperature sensitivity of the reaction rate is predominantly determined by the activation energy, obtaining reliable estimates for this parameter is especially critical for predicting thermal stabilities.[4]

Heating of AN results in complete conversion of the material into gases. Kinetic characteristics of AN gassification have been estimated by several workers.[5−18] The reported values are collected in Table 1. Although the majority of workers assumed the same kinetic model (first-order reaction), the resulting activation energies do not agree with each other, spanning a factor of ∼7. It is noteworthy that previous kinetic studies appear to have been primarily concerned with the liquid-state processes. Our literature search did not show any studies that specifically address the kinetics of thermally stimulated processes in solid AN. Obtaining this information is vital for practical purposes such as estimating the thermal stability and/or shelf life of the solid AN.

In the present work we systematically study the kinetics of gassification of solid and liquid AN. Our study focuses on estimating reliable kinetic characteristics. As shown earlier, the estimates based on fitting data to single-step kinetic models tend to be misleading, especially when these estimates are obtained from nonisothermal measurements.[19,20] As an alternative, one may use model-free isoconversional methods that allow for reliably estimating the activation energy as a function of the extent of conversion. The resulting dependence can effectively be used for drawing a mechanistic conclusion as well as for performing kinetic predictions.[19,20] In this study, both model-fitting and

(1) Russel, T. P.; Brill, T. B. *Combust. Flame* **1989**, *76*, 393.
(2) Brill, T. P.; Brush, P. J.; Patil, D. G. *Combust. Flame* **1993**, *92*, 178.
(3) Pasternack, L.; Rice, J. K. *J. Phys. Chem* **1993**, *97*, 12805.
(4) Vyazovkin, S.; Linert, W. *Anal. Chim. Acta* **1994**, *295*, 101.
(5) Robertson, A. J. *J. Soc. Chem. Ind.* **1948**, *67*, 221.
(6) Hainer, R. M. *Fifth International Symposium on Combustion, 1954*; Reinhold: New York, 1955; p 224.
(7) Wood, B. J.; Wise, H. *J. Chem. Phys.* **1995**, *23*, 693.
(8) Cook, M. A.; Abegg, M. T. *Ind. Eng. Chem.* **1956**, *48*, 1090.
(9) Andersen, W. H.; Bills, K. W.; Dekker: A. O.; Mischuck, E.; Moe, G.; Schultz, R. D. *Jet Propul.* **1958**, *28*, 831.
(10) Guiochon, G. *Ann. Chim.* **1960**, *5*, 295.
(11) Keenan, A. G.; Dimitriades, B. *J. Chem. Phys.* **1962**, *37*, 1019.
(12) Rosser, W. A.; Inami, S. H.; Wise, H. *J. Phys. Chem.* **1963**, *67*, 1753.
(13) Dobychin, S. L.; Smirnov, V. M. *J. Appl. Chem. USSR* **1963**, *36*, 199.
(14) Brower, K. R.; Oxley, J. C.; Tewari, M. *J. Phys. Chem.* **1989**, *93*, 4029.
(15) Koga, N.; Tanaka, H., *Thermochim. Acta* **1992**, *209*, 127.
(16) Koga, N.; Tanaka, H., *Thermochim. Acta* **1994**, *240*, 141.
(17) Koroban, V. A.; Burtsev, Yu. N.; Alimov, F. R.; Haustov, A. D.; Dubovik, V. A.; Teselkin, V. A. *Propellants, Explos., Pyrotech.* **1994**, *19*, 307.
(18) Carvalheira, P.; Gadiot, G. M. H. J. L.; de Klerk, W. P. C. *Thermochim. Acta* **1995**, *269/270*, 273.
(19) Vyazovkin, S.; Wight, C. A. *Int. Rev. Phys. Chem.* **1998**, *17*, 407.
(20) Vyazovkin, S.; Wight, C. A. *Thermochim. Acta* **1999**, *340/341*, 53.

10.1021/cm000708c CCC: $20.00
Published on Web 02/10/2001

Table 1. Literature Values of the Arrhenius Parameters for the Thermal Gassification of AN

measurement	mass	*p*, atm	*T*-region, °C	kinetic eq	*E*, kJ mol^{-1}	log(*A*/s^{-1})	ref
pressure vs time, isothermal	2-123 mg	1	243−300	1st order	169	13.8	5
mass vs time, isothermal	300 g	-	220−290	1st order	∼200	>14	6
[HNO_3], [NH_3] vs time, isothermal	-	vacuum	170−280	1st order	131	14.2	7
mass vs time, isothermal	0.05−0.25 g	1	218−267	1st order	160	12.3	8
linear pyrolysis rate vs temperature	-	1	180−300	0th order	30	-	9
mass vs time, isothermal	0.05−6 g		170−280	1st order	153	11.5	10
[N_2O] vs time, isothermal	100 g		230−265	1st order	207	16.5	11
[N_2O] vs time, isothermal	10 g	1	225−275	1st order	171	15.7	12
[NO_2], [NH_3] vs time	100 mg	vacuum	170−200	-	53	-	13
[N_2O] vs time, isothermal	1-4 mg	vacuum	200−380	1st order	118−193[a]	-	14
mass vs time, isothermal	3-15 mg	1	170−210	$\alpha = kt$	86[b]	6.7[b]	15
mass vs temperature, nonisothermal	5-15 mg	1	140−220	ln(dα/dt) vs $1/T_\alpha$	94[b]	7.0[b]	16
ΔT vs temperature, nonisothermal (DTA)	1-5 mg	1	270−320	0th order	138	10.3	17
mass vs temperature, nonisothermal	10-11 mg	1	150−300	1st order	114	8.5	18

[a] *E* increases with *T*. [b] Average value

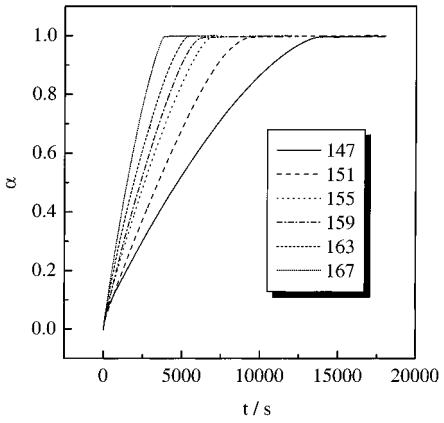

Figure 1. Isothermal kinetic curves for the solid-state gassification of AN. The temperature of the experiment (in °C) is indicated by each line.

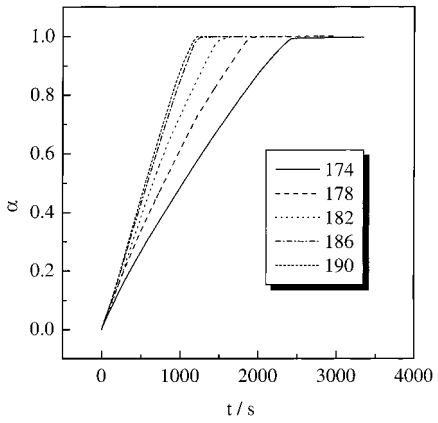

Figure 2. Isothermal kinetic curves for the liquid-state gassification of AN. The temperature of the experiment (in °C) is indicated by each line.

model-free computational techniques are applied to the thermal conversion of AN under isothermal and nonisothermal conditions.

Experimental Section

Ammonium nitrate (AN) of 99.8% purity (Mallinckrodt) was used with no further purification. The samples were ground up in an agate mortar. The particle size was <300 μm, as measured by using an optical microscope. A Mettler-Toledo TGA/SDTA851^e module was used to measure the mass loss kinetics under both isothermal and nonisothermal conditions. To compare the solid- and liquid-phase kinetics, the isothermal TGA runs were carried out below and above the melting point (T_m = 169.5 °C)[21] at temperatures 147, 151, 155, 159, 163, 167, 174, 178, 182, 186, and 190 °C (Figures 1 and 2). Two isothermal DSC experiments were run at 167 and 174 °C. The isothermal measurements were started after a short warm-up period (∼ 40 s). Additionally, five nonisothermal TGA and DSC runs were conducted at heating rates of 2.5, 5, 7.5, 10, and 12.5 °C min^{-1} (Figure 3). The DSC runs were performed by using a Mettler-Toledo DSC821^e module. In all experiments, AN samples of ∼1 mg were heated in open 40 μL Al pans in a flowing atmosphere of nitrogen at a flow rate 70 mL min^{-1}.

Kinetic Computations

Kinetic analysis of solid state reactions is usually based on a single-step kinetic equation[22,23]

$$\frac{d\alpha}{dt} = k(T)\, f(\alpha) \qquad (1)$$

where t is the time, α is the extent of conversion, $k(T)$ is the rate constant, and $f(\alpha)$ is the reaction model associated with a certain mechanism. The temperature dependence of the rate constant is traditionally presented by the Arrhenius equation

$$k(T) = A \exp\left(\frac{-E}{RT}\right) \qquad (2)$$

where A (the preexponential factor) and E (the activation energy) are the Arrhenius parameters and R is the gas constant. At any moment of time, TGA allows one to determine α as a partial mass loss. The direct application of eq 2 to TGA data requires numerical differentiation of experimental measurements. However, this procedure typically produces unacceptably noisy data. This situation is effectively avoided by using eq 1 in its integral form. Some of the integral methods are described below.

Model Fitting Method for Isothermal Data. Rearrangement and integration of eq 1 for isothermal conditions gives

$$g(\alpha) = \int_0^\alpha \frac{d\alpha}{f(\alpha)} = k(T)t \qquad (3)$$

(21) *CRC Handbook of Thermophysical and Thermochemical Data*; Lide, D. R.; Kehiaian, H. V., Eds.; CRC Press: Boca Raton, 1994.
(22) Brown, M. E.; Dollimore, D.; Galwey, A. K. *Reactions in the Solid State* in *Comprehensive Chemical Kinetics*; Bamford, H.; Tipper, C. F. H., Eds.; Elsevier: Amsterdam, 1980; Vol. 22.
(23) Galwey, A. K.; Brown, M. E. *Thermal Decomposition of Ionic Solids;* Elsevier: Amsterdam, 1999.

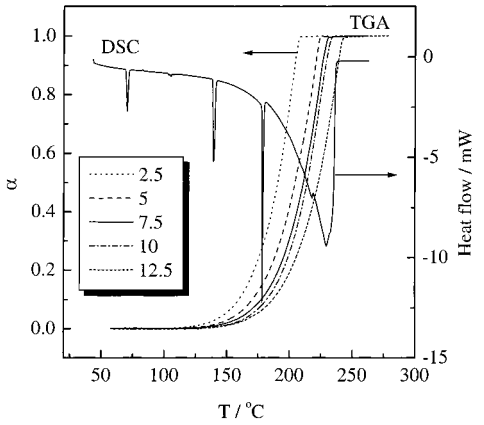

Figure 3. Nonisothermal kinetic curves and a typical DSC trace. The heating rate of the experiment (in °C min^{-1}) is indicated by each line.

where $g(\alpha)$ is the integral form of the reaction model (Table 2). To choose an appropriate reaction model, one can plot α as a function of a reduced time variable t/t_α, where t_α is the time required to reach a specified conversion (e.g., $\alpha = 0.9$). The method is widely used in solid-state kinetics.[22,23] Once the reaction model is determined, the rate constant can be estimated from the slope of a plot of $g(\alpha)$ versus t (eq 3). For each reaction model selected, the rate constants are evaluated at several temperatures, T_i, and the Arrhenius parameters are determined in the usual manner using the Arrhenius equation in its logarithmic form

$$\ln k(T_i) = \ln A - \frac{E}{RT_i} \tag{4}$$

Confidence intervals for Arrhenius parameters are determined with the help of the standard statistical procedure of linear regression analysis.[24,25]

Model Fitting Method for Nonisothermal Data. Nonisothermal runs are usually performed at a constant heating rate

$$\beta = \frac{\mathrm{d}T}{\mathrm{d}t} \tag{5}$$

With regard to eq 5, rearrangement and integration of eq 1 gives

$$g(\alpha) = \frac{A}{\beta}\int_0^{T_\alpha} \exp\left(\frac{-E}{RT}\right)\mathrm{d}T \tag{6}$$

Various approximations of the temperature integral in eq 6 are used to arrive at simple equations suitable for evaluating Arrhenius parameters.[22,23,26] One such approximation gives rise to the popular Coats−Redfern equation[27]

$$\ln\left[\frac{g_j(\alpha)}{T^2}\right] = \ln\left[\left(\frac{A_jR}{\beta E_j}\right)\left(1 - \frac{2R\bar{T}}{E_j}\right)\right] - \frac{E_j}{RT} \tag{7}$$

where $\bar{T}$ is the mean experimental temperature. Inserting various $g_j(\alpha)$ into eq 7 results in a set of Arrhenius parameters determined from the plot $\ln[g_j(\alpha)/T^2]$ against T^{-1}. This equation as well as a number of other similar equations is customarily used for kinetics analysis of thermoanalytical measurements conducted at a single heating rate. The sets of Arrhenius parameters for the thermal conversion of AN are shown in Table 2. Confidence intervals are estimated by using the standard statistical procedure of linear regression analysis.[24,25] The goodness of fit is estimated by a coefficient of linear correlation, r_j.

Model-Free Isoconversional Method for Isothermal and Nonisothermal Data. Flynn and Wall[28] and Ozawa[29] developed the first integral isoconversional methods for evaluating the activation energy from a series of thermoanalytical experiments conducted at several heating rates. These methods assume that the reaction model, $g(\alpha)$ is independent of the heating rate. Analysis of measurements related to a given extent of conversion at different heating rates allows one to eliminate the analytical form of the reaction model from evaluations of the activation energy. The methods of Flynn and Wall and Ozawa can only be applied to the kinetics measured at constant heating rates. Vyazovkin[30] proposed an advanced isoconversional method which is applicable to the data obtained at arbitrary heating programs, $T(t)$. For such conditions integration of eq 1 gives

$$g(\alpha) \equiv \int_0^\alpha \frac{\mathrm{d}\alpha}{f(\alpha)} = A\int_0^{t_\alpha} \exp\left(\frac{-E}{RT(t)}\right)\mathrm{d}t = AJ[E,T(t_\alpha)] \tag{8}$$

whence the subscript α denotes the values related to a given extent of conversion. By assuming that the reaction model is independent of the heating program, one can equate the right-hand sides of eq 8 for different heating programs. Then for a set of n experiments carried out at different heating programs, the activation energy is determined at any particular value of α by finding E_α, which minimizes the function

$$\Phi(E_\alpha) = \sum_{i=1}^{n}\sum_{j\neq i}^{n}\frac{J[E_\alpha,T_i(t_\alpha)]}{J[E_\alpha,T_j(t_\alpha)]} \tag{9}$$

where the subscripts i and j represent oridinal numbers of two experiments performed under different heating programs. The integral J in eq 9 is evaluated numerically by using the trapezoid rule. The minimization procedure is repeated for each value of α to find the dependence of the activation energy on the extent of conversion. The method has been successfully applied to thermoanalytical data to elucidate the kinetics and the mechanism of processes occurring in inorganic and polymeric materials.[31−33] The method is easily modified to more adequately account for a variation of the activation energy with the extent of conversion.[34] This is accomplished by breaking the kinetic curves up into

(24) Johnson, N. L.; Leone, F. C. *Statistics and Experimental Design in Engineering and the Physical Sciences;* J. Wiley & Sons: New York, 1977; Vol. 1.
(25) Massart, D. L.; Vandeginste, B. G. M.; Buydens, L. M. C.; de Jong, S.; Lewi, P. J.; Smeyers-Verbke, J. *Handbook of Chemometrics and Qualimetrics;* Elsevier: Amsterdam, 1997; Part A.
(26) Flynn, J. H. *Thermochim. Acta* **1997**, *300*, 83−92.
(27) Coats, A. W.; Redfern, J. P. *Nature* **1964**, *201*, 68.
(28) Flynn, J. H.; Wall, L. A. *J. Res. Nat. Bur. Standards A* **1966**, *70*, 487.
(29) Ozawa, T. *Bull. Chem. Soc. Jpn.* **1965**, *38*, 1881.
(30) Vyazovkin, S. *J. Comput. Chem.* **1997**, *18*, 393.

Table 2. Activation Energies for Gassification of AN at 5 °C min^{-1} Determined Using the Coats−Redfern Eq 5

N	reaction model	g(α)	E/kJ mol^{-1}	log(A/min^{-1})	$\|r\|$
1	power law	$\alpha^{1/4}$	11.5 ± 0.1	0.2 ± 0.0	0.9670
2	power law	$\alpha^{1/3}$	17.7 ± 0.2	0.6 ± 0.0	0.9749
3	power law	$\alpha^{1/2}$	30.1 ± 0.3	2.0 ± 0.0	0.9803
4	power law	$\alpha^{3/2}$	104.5 ± 0.8	10.2 ± 0.1	0.9851
5	one-dimensional diffusion	α^2	141.6 ± 1.0	14.2 ± 0.1	0.9856
6	Mampel (first order)	$-\ln(1-\alpha)$	81.5 ± 0.6	8.2 ± 0.1	0.9824
7	Avrami−Erofeyev	$[\ln(1-\alpha)]^{1/4}$	15.1 ± 0.2	0.4 ± 0.0	0.9722
8	Avrami−Erofeyev	$[\ln(1-\alpha)]^{1/3}$	22.5 ± 0.2	1.3 ± 0.0	0.9766
9	Avrami−Erofeyev	$[\ln(1-\alpha)]^{1/2}$	37.2 ± 0.3	3.1 ± 0.0	0.9799
10[a]	three-dimensional diffusion	$[1-(1-\alpha)^{1/3}]^2$	156.7 ± 1.0	15.3 ± 0.1	0.9875
11[a]	contracting sphere	$1-(1-\alpha)^{1/3}$	74.8 ± 0.5	6.8 ± 0.1	0.9865
12[a]	contracting cylinder	$1-(1-\alpha)^{1/2}$	72.4 ± 0.5	6.6 ± 0.1	0.9866

[a] Statistically equivalent models.

segments. The activation energy for each segment is determined from numerical integration of the $T(t)$ data over the segment

$$J[E_\alpha, T_j(t_\alpha)] \equiv \int_{t_{\alpha-\Delta\alpha}}^{t_\alpha} \exp\left[\frac{-E_\alpha}{RT_i(t)}\right] dt \qquad (10)$$

In eq 10 α varies from 2Δα to 1 − Δα with a step Δα = $(m+1)^{-1}$, where m is the number of the α values chosen for the analysis (typically 10−50). In this work the advanced isoconversional method is applied to both isothermal and nonisothermal data on gassification of AN.

Confidence Intervals for the Advanced Isoconversional Method. Confidence intervals have been estimated by using a special statistical procedure.[35] By virtue of the basic assumption that the reaction model, $g(\alpha)$, is independent of the heating program, $T(t)$, the J-integrals (eq 10) for any particular segment ($t_{\alpha-\Delta\alpha} - t_\alpha$) should be equal for all experiments, regardless of differences in the heating programs (cf., eq 8). Therefore, the ratio of any two of the J-integrals should be unity in an ideal situation. It is noteworthy that for any set of n experiments, the total number of terms contributing to the double summation (eq 9) is $n(n-1)$. Then the following variance

$$S^2(E_\alpha) = \frac{1}{n(n-1)} \sum_{i=1}^{n} \sum_{j \neq i}^{n} \left(\frac{J[E_\alpha, T_i(t_\alpha)]}{J[E_\alpha, T_j(t_\alpha)]} - 1 \right)^2 \qquad (11)$$

should be independent of the number of experiments performed (aside from the natural fluctuations associated with experimental values themselves). Minimization of this variance yields an optimum value of the activation energy, $E_{\min}$, which is characterized by the minimum variance, $S^2_{\min}$. Then, statistics constructed as

$$\Psi(E_\alpha) = \frac{S^2(E_\alpha)}{S^2_{\min}} \qquad (12)$$

have the F-distribution.[24,25] This enables the confidence limits for $E_{\min}$ to be found by estimating the confidence limits for the variance $S^2_{\min}$. The p × 100% confidence interval for $S^2_{\min}$ can be determined from the following condition

$$\Psi(E_\alpha) < F_{1-p,n-1,n-1} \qquad (13)$$

where $F_{1-p,n-1,n-1}$ is a percentile of the F-distribution for the (1 − p) × 100% confidence probability. Then for $E_\alpha{}^{\min}$, we can estimate the lower and upper confidence limit ($E_\alpha{}^{lo}$ and $E_\alpha{}^{up}$, respectively) as the values of E_α for which $\Psi(E_\alpha) = F_{1-p,n-1,n-1}$ (Figure 4).

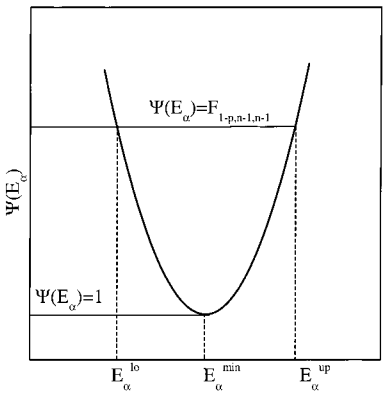

Figure 4. Illustration of the statistical procedure of estimating confidence limits.

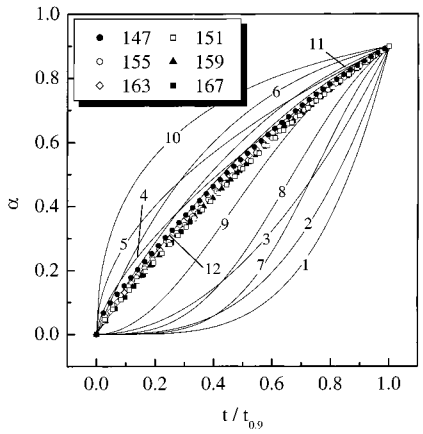

Figure 5. Reduced time plots for the solid-state gassification of AN. The temperature of the experiment (in °C) is indicated by respective points.

Results and Discussions

Model-Fitting Analysis. Figure 5 shows the reduced time plots for the isothermal gassification of solid AN. The plots related to different temperatures are practically identical. Although no model describes the experi-

(31) Peterson, J. D.; Vyazovkin, S.; Wight, C. A. *J. Phys. Chem. B* **1999**, *102*, 8087.
(32) Vyazovkin, S.; Wight, C. A. *Chem. Mater.* **1999**, *11*, 3386.

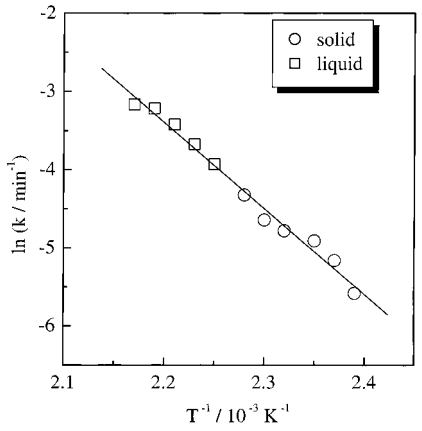

Figure 6. Arrhenius plot for the isothermal gassification of AN. The solid- and liquid-phase processes are respectively represented by circles and squares.

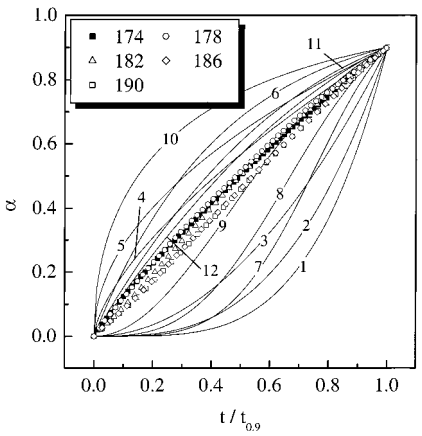

Figure 7. Reduced time plots for the liquid-state gassification of AN. The temperature of the experiment (in °C) is indicated by respective points.

mental data perfectly, the model of contracting cylinder (model 12) appears to be a very close match. This model was employed for estimating the rate constants. The resulting Arrhenius plot is depicted in Figure 6.

The reduced time plots for the isothermal gassification of liquid AN are displayed in Figure 7. As we can see, the three plots corresponding to temperatures 174, 178, and 182 °C coincide fairly well. The plots corresponding to higher temperatures 186 and 190 °C show some deviation from the plots obtained at the lower temperatures. The deviation is likely to be caused by the initial warm-up period during which the sample reaches the preset isothermal temperature. Because at higher temperatures the process proceeds faster, the sample may undergo a noticeable gassification during the warm-up period. As a result, the kinetic curves have a systematic shift that increases with temperature.

Since some of the reaction models are exclusively applicable to solid-state processes, a comparison of the liquid-phase data against them would not be meaningful for mechanistic purposes. It should, however, be noted that the models such as the first-order reaction (N6) and autocatalytic models (N7−9) can be used to describe the liquid-phase kinetics as well as the contracting geometry models (N11 and N12) may be applicable to vaporization kinetics. At any rate, the obtained reduced time plots for the liquid-state gassification are suitable for a comparison with the respective plots obtained for the solid-state process. By comparing the reduced time plots obtained for the solid- and liquid-phase gassifications, we can see that they look quite similar. Although no kinetic model provides a perfect match for the liquid-phase gassification data, the contracting cylinder model (N12) still appears to be the best match. Contrary to the common assumption, the liquid-phase gassification does not follow first-order kinetics (cf., Table 1). The model of a contracting cylinder has been used to derive the rate constants for the thermal gassification of liquid AN. The respective Arrhenius plot is shown in Figure 6.

The Arrhenius plots related to the solid- and liquid-phase gassification form a single straight line (Figure 6) that is characterized by a coefficient of linear correlation 0.9959. From this line we obtain the activation energy of 91.5 ± 5.6 kJ mol^{-1} and $\log(A/\text{min}^{-1}) = 9.0 \pm 0.6$.

The nonisothermal runs cover both solid- and liquid-phase gassifications (Figure 3). As follows from the isothermal data analysis, the gassification kinetics do not demonstrate any apparent difference for the two phases. It does not, therefore, seem unreasonable to attempt describing the whole process with a single pair of Arrhenius parameters. The application of the model-fitting method to a single-heating rate nonisothermal data results in Arrhenius parameters that exhibit a strong dependence on the reaction model chosen (Table 2). Most of the models give rise to good linear fits as characterized by the values of *r*. Although the maximum of the absolute value of the linear correlation coefficients falls on model 12, statistical analysis based on Fisher's transformation[20,24,25] suggests that this model cannot be differentiated from models 10 and 11 with a 95% confidence probability. Note that the activation energies related to these equivalent models span a factor of 2.

The large uncertainty in the Arrhenius parameters is typically observed[19,20] when one attempts to simultaneously fit the temperature and conversion terms (i.e., k(T) and $f(\alpha)$, respectively) of eq 1 (or its integral variant) to rate data of a single nonisothermal run. Because in a nonisothermal experiment T and α vary at the same time, the simultaneously fitted $k(T)$ and $f(\alpha)$ terms are unavoidably correlated, giving rise to a strong mutual correlation between log A and E.[20] Also known as a kinetic compensation effect, this correlation belongs to a large family of false isokinetic relationships.[36] Figure 8 provides a vivid example of a compensation effect for gassification of ammonium nitrate. It is seen that the correlation line includes all the Arrhenius parameters determined by fitting various reaction models to a nonisothermal experiment (Table 2). Although the obtained parameters are too uncertain to be sound, the compensation effect may nevertheless have some practical use because it necessarily includes the correct values of Arrhenius parameters.[37] For instance,

(33) Vyazovkin, S.; Sbirrazzuoli, N. *Macromol. Chem. Phys.* **2000**, *201*, 199.
(34) Vyazovkin, S. *J. Comput. Chem.* **2001**, 22, 178.
(35) Vyazovkin, S.; Wight, C. A. *Anal. Chem.* **2000**, *72*, 3171.
(36) Vyazovkin, S.; Linert, W. *Int. Rev. Phys. Chem.* **1995**, *14*, 355.
(37) Vyazovkin, S.; Linert, W. *Chem. Phys.* **1995**, *193*, 109.

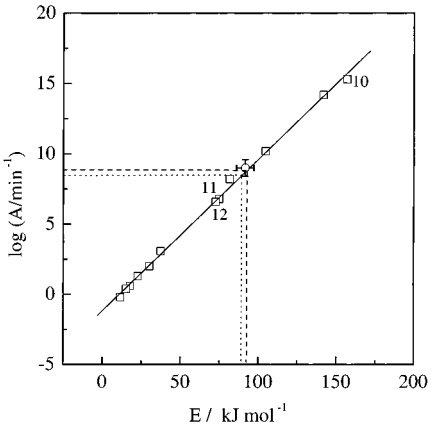

Figure 8. Compensation effect observed for the nonisothermal gassification of AN. Squares represent the Arrhenius parameters estimated by using reaction models (Table 2). The numbers are shown for the "best" reaction models. The circle with error bars corresponds to the Arrhenius parameters derived from isothermal experiments. Dotted and dashed lines illustrate the procedure of estimating preexponential factors in isoconversional computations.

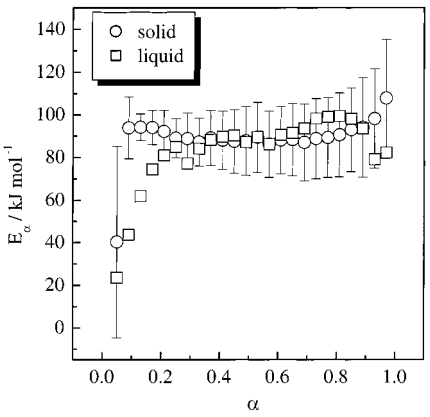

Figure 9. Dependencies of the activation energy on the extent of conversion determined by the isoconversional method for the solid (circles) and liquid (squares) state gassification under isothermal conditions.

the Arrhenius parameters estimated from the isothermal measurement also belong to this line (Figure 8).

Model-Free Analysis. The advanced isoconversional method has been applied to the gassification data of AN to obtain the dependencies of the activation energy on the extent of conversion. Figure 9 shows the E_α-dependencies for the isothermal gassification of AN. The solid-state gassification is characterized by an activation energy that is practically independent of the extent of conversion. The constancy of the activation energy indicates that the overall kinetics is likely to be governed by a single reaction step. For the region of $\alpha = 0.1-0.9$, the average activation energy is 89.4 ± 0.8 kJ mol^{-1}. For gassification in the liquid state, the activation energy demonstrates an increase at $\alpha < 0.2$. At greater extents of conversion, the activation energy of the liquid-state gassification agrees well with the activation energy for the solid-state process. The initial increase in E_α for the liquid-state process is speculated to result from the systematic error caused by sample gassification during the warm-up period (vide supra). If this increase is associated with changes in the reaction mechanism, we should also observe a change in the activation energy

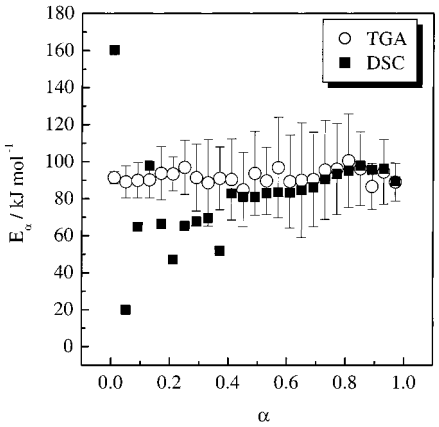

Figure 10. Dependencies of the activation energy on the extent of conversion determined by the isoconversional method from the nonisothermal TGA (circles) and DSC (squares) data.

to occur for the nonisothermal gassification when sample undergoes melting.

Figure 10 displays the E_α-dependencies for the nonisothermal gassification of AN. As seen from Figure 3, at $\alpha < 0.1$ the gassification occurs in the solid state. However, the respective portion of the E_α-dependence does not show an apparent difference from the part corresponding to the liquid-state gassification. This fact is consistent with our speculation that the initial increase in E_α for the liquid-state isothermal gassification (Figure 9) is an artifact. The activation energy for the nonisothermal gassification does not seem to show any systematic variation throughout the whole interval of conversions. The average value is 92.7 ± 1.2 kJ mol^{-1}, which is in good agreement with the values obtained from the isothermal experiments (Figure 9).

Because the compensation effect of the type shown in Figure 8 is known[37] to include the correct values of Arrhenius parameters, it can be used[38,39] for estimating the preexponential factor in the isoconversional computations. In particular, the compensation effect shown in Figure 8 has the following functional form

$$\log A = 0.108E - 1.17 \qquad (14)$$

By substituting the values of E determined by the isoconversional method into eq 14, one can obtain estimates for the preexponential factor (see Figure 8). In this manner, we obtain the values of $\log(A/\text{min}^{-1}) = 8.5$ and 8.8 for the above-mentioned values of $E = 89.4$ and 92.7 kJ mol^{-1}, respectively.

For comparison purposes, we have also extracted the E_α-dependence from the DSC data. The resulting dependence is presented in Figure 10. The strong scatter in the E_α values at $\alpha < 0.4$ is caused by the sharp changes in the DSC signal that are associated with the tetragonal to cubic transition (125.4 °C) and melting (169.5 °C). At $\alpha > 0.4$, the E_α-dependence is in good agreement with the dependence estimated from the TGA measurements. Therefore, both TGA and DSC methods appear to measure similar kinetics. The average reaction heat measured by integration of the DSC data is 198 ± 16 kJ mol^{-1}, which is reasonably consis-

(38) Vyazovkin, S. *Int. J. Chem. Kinet.* **1996**, *28*, 95.
(39) Vyazovkin, S.; Wight, C. A. *Annu. Rev. Phys. Chem.* **1997**, *48*, 125.

tent with the thermodynamic estimate 184 kJ mol^{-1} for the following reaction at 25 °C

$$NH_4NO_3(s) \leftrightarrow NH_3(g) + HNO_3(g) \qquad (15)$$

For liquid AN, the endothermicity of this reaction is decreased by the heat of AN fusion, which is 6.2 kJ mol^{-1}.[21] Manelis et al.[40] stress that the actually measured heat may also involve the heats of evaporation of ammonia and nitric acid dissolved in AN. According to their estimates, the respective heats are about 24 and 26 kJ mol^{-1}.

Interpretation of Results. The major finding of the above kinetic analyses is that the thermal gassification of AN demonstrates similar kinetic regularties in the solid and liquid phase. For both phases, the model-free kinetic analysis yeilds an activation energy of around 90 kJ mol^{-1}, which is essentially independent of the extent of conversion. It is, therefore, reasonable to assume that the gassification kinetics are determined by a common single reaction step in both phases. This assumption is also consistent with the results of the model-fitting analysis. When applied to the isothermal data, it shows that both solid- and liquid-state gassification are described by a single activation energy of about 90 kJ mol^{-1} and by the same reaction model of a contracting cylinder.

The experimentally determined value of the reaction heat suggests that the thermal gassification occurs predominantly via dissociative sublimation/vaporization (eq 15). The latter is known to overlap with an exothermic (54 kJ mol^{-1}) channel

$$NH_4NO_3(s) \rightarrow N_2O + 2H_2O \qquad (16)$$

which occurs as a series of secondary reactions of ammonia and nitric acid.[7,12,14] The rate measurements based on the concentration of N_2O give the following values of the activation energies for the exothermic channel: 207,[11] 171,[12] and 118[14] kJ mol^{-1} (Table 1). While not mutually consistent, these values are apparently greater than the activation energy found in the present study. The significant presence of the exothermic channel with a greater activation energy would likely cause a noticeable change in the activation energy with the temperature and/or the extent of conversion. Because this channel is exothermic, its significant contribution would also cause a noticeable decrease of the overall reaction endothermicity as compared with the thermodynamic estimates for reaction 15. Neither of these effects have been observed in the present study. Therefore, the kinetic characteristics reported in the present study should be assigned to the process of the dissociative sublimation/vaporization of AN.

It may appear somewhat unusual that the activation energy for the endothermic reaction 15 is much smaller than the reaction enthalpy. A similar result was reported by Jacobs and Russel-Jones,[41] who found the activation energy for sublimation of ammonium perchlorate to be half the reaction enthalpy. Generally, this effect is not unsual for sublimation of solids.[42] An explanation to this effect is provided by a model of stepwise vaporization.[42] This model has been applied by Aleksandrov and Khairetdinov[43] to explain the difference between the activation energy and the enthalpy of sublimation of ammonium perchlorate.

The model-fitting analysis of the isothermal data suggests that in both phases the gassification kinetics follow the model of a contracting cylinder. The contracting surface models describe the kinetics of a process that occurs on the surface and whose rate is determined by the surface-to-volume ratio. These models were found to adequately describe the kinetics of sublimation of various solids,[22,23] including ammonium perchlorate.[41] Inasmuch as these models apply to sublimation of crystals of various shapes, they can also be used to describe the kinetics of vaporization of a liquid in the form of droplets. It is not, therefore, surprising that the same reaction model holds for sublimation and vaporization of AN.

Conclusions

The thermal gassification of AN demonstrates silmilar kinetics in the solid and liquid phase. In both phases, the process can be described by the activation energy of ~90 kJ mol^{-1}, by the preexponential factor of around 10^9 min^{-1}, and by the reaction model of a contracting cylinder. These kinetic charactersitics are assigned to the process of dissociative sublimation/vaporization.

Acknowledgment. The authors thank the Mettler-Toledo, Inc. for donating the TGA and DSC instruments used in this study. Support for this work from the Ballistic Missile Defense Organization and the Office of Naval Research under MURI contract No. N00014-95-1-1339 and from the University of Utah Center for Simulations of Accidental Fires and Explosions, funded by the Department of Energy, Lawrence Livermore Laboratory, under subcontract B341493, is gratefully acknowledged.

Note Added after ASAP Posting

This article was released ASAP on 2/10/01 with an error in eq 11. The correct version was posted on 2/15/01.

CM000708C

(40) Manelis, G. B.; Rubtsov, Yu. I.; Raevskii, A. V. *Combust. Explos. Shock Waves* **1970**, *6*, 1.

(41) Jacobs, P. W. M.; Russel-Jones, A. *J. Phys. Chem.* **1968**, *72*, 202.

(42) Samorjai, G. A.; Lester, J. E. *Prog. Solid State Chem.* **1967**, *4*, 1.

(43) Alexandrov, V. V.; Khairetdinov, E. F. *Kinet. Katal.* **1971**, *12*, 1327.